processes

MDPI

Article

Enhancing the Photoelectric Properties of Flexible Carbon Nanotube Paper by Plasma Gradient Modification and Gradient Illumination

Chen-Chen Yang [1], Pi-Yu Shen [1], Hsin-Yuan Miao [1], Chia-Yi Huang [2], Shih-Hung Lin [3], Jun-Hong Weng [1], Lakshmanan Saravanan [4] and Jih-Hsin Liu [1,*]

[1] Department of Electrical Engineering, Tunghai University, Taichung 407, Taiwan; g11360002@thu.edu.tw (C.-C.Y.); thusemidevice@gmail.com (P.-Y.S.); kenymiao@thu.edu.tw (H.-Y.M.); jhw@thu.edu.tw (J.-H.W.)
[2] Department of Applied Physics, Tunghai University, Taichung 407, Taiwan; chiayihuang@thu.edu.tw
[3] Department of Electronic Engineering, National Yunlin University of Science and Technology, 123 University Road, Section 3, Douliou 640, Taiwan; isshokenmei@yuntech.edu.tw
[4] Department of Physics, Saveetha School of Engineering, Saveetha Institute of Medical and Technical Sciences, Saveetha University, Chennai 602105, India; ljsaravanan08@gmail.com
* Correspondence: jhliu64@thu.edu.tw

Abstract: This study investigates the impact of plasma gradient modification and gradient illumination on the optoelectronic properties of buckypaper (BP), a flexible and large-scale material composed of multi-walled carbon nanotubes (MWCNTs). The BP samples were subjected to argon ion plasma treatment at varying power levels and durations, thereby creating different carrier concentration gradients on the surface. The photovoltage and photocurrent responses of the samples were then measured under uniform full illumination and gradient illumination conditions. The findings revealed that both plasma gradient modification and gradient illumination significantly enhanced the optoelectronic performance of BP. Notably, the combined application of these two methods yielded superior results compared to the application of either method alone. Specifically, the optimal plasma power for improving BP was found to be 20 W. Under conditions of plasma gradient modification and gradient illumination, a photovoltage of 267.76 μV was generated, which represents a 21.44 times increase, and a photocurrent of 15.69 μA, reflecting a 32.69 times enhancement. The mechanism underlying this optoelectronic effect can be attributed to the presence of π-bonds in the carbon atoms. These π-bonds are excited by photons, resulting in the generation of small voltages and currents. This study underscores the potential of BP as an optoelectronic material and introduces a novel approach to enhance its optoelectronic properties through plasma gradient modification and gradient illumination.

Keywords: carbon nanotube; plasma; optoelectronic material; gradient illumination

Citation: Yang, C.-C.; Shen, P.-Y.; Miao, H.-Y.; Huang, C.-Y.; Lin, S.-H.; Weng, J.-H.; Saravanan, L.; Liu, J.-H. Enhancing the Photoelectric Properties of Flexible Carbon Nanotube Paper by Plasma Gradient Modification and Gradient Illumination. *Processes* **2024**, *12*, 1449. https://doi.org/10.3390/pr12071449

Academic Editor: Jia Huo

Received: 11 June 2024
Revised: 8 July 2024
Accepted: 9 July 2024
Published: 11 July 2024

1. Introduction

Carbon nanotubes (CNTs) are one-dimensional nanostructures exhibiting exceptional electrical, mechanical, and optical properties. Since their discovery by Sumio Iijima in 1991 [1], CNTs have garnered extensive attention for their potential applications in various fields such as nanoelectronics, sensors, solar cells, and flexible devices [2–4]. For instance, Liu et al. experimented with doping the elements boron and phosphorus on opposite sides of carbon nanotube paper to fabricate flexible components exhibiting PN diode characteristics. These components can adjust their absorption frequency through the application of a direct current bias, thereby serving as novel electromagnetic wave-absorbing materials [5]. A notable characteristic of CNTs is their photoelectric response, which refers to the generation of current and voltage upon exposure to light. This phenomenon has been observed in both single-walled and multi-walled carbon nanotubes (SWCNTs and MWCNTs) and is attributed to the excitation and mobility of π-electrons within the CNTs [6,7].

Nevertheless, the photoelectric performance of CNTs is often constrained by several factors, including low light absorption efficiency, high contact resistance, and the recombination of photogenerated carriers. Consequently, various strategies have been proposed to enhance the photoelectric response of CNTs, such as doping, functionalization, hybridization, and device engineering [8–11]. In the seminal experiments conducted by Liu et al., an initial attempt was made to enhance the photovoltage by doping titanium dioxide into black phosphorus (BP), which resulted in an increase from 13 microvolts to 30 microvolts. Subsequently, by substituting the dopant with copper oxide, the photovoltage further escalated to 57 microvolts [12]. Over the course of several years, the researchers refined their methodology by opting for zinc oxide as the dopant and implementing an annealing process, culminating in a significant elevation of the photovoltage from 18.3 microvolts to 74.49 microvolts [13]. Conversely, Wang et al. incorporated silver nanoparticles into BP, leading to an enhancement of the photovoltage from 10.12 microvolts to 23.26 microvolts [14].

Additionally, plasma treatment has been identified as a straightforward yet efficacious method for modifying the surface and structure of carbon nanotubes. This treatment introduces defects, impurities, and dopants, thereby augmenting their performance [15]. According to studies, oxygen plasma treatment can significantly alter the surface chemistry of carbon nanotubes. Xu and colleagues observed that oxygen plasma treatment could completely purify multi-walled carbon nanotubes (MWCNTs) within 30 min, introducing oxygen-containing functional groups on their surface, thereby markedly enhancing their reactivity. Specifically, after plasma treatment, the content of sp^3 carbon on the surface of MWCNTs decreased from 23.8% to 5.0%, while the oxygen content increased from 1.6% to 16.6%. This indicates that the oxygen plasma effectively removes the amorphous carbon layer on the surface of the carbon nanotubes and introduces functional oxygen groups, thus improving their chemical reactivity and dispersibility [16].

Moreover, plasma treatment can also modify the ratio of sp^2 to sp^3 bonds in carbon nanotubes, thereby regulating their electronic and photoelectronic properties. Such modifications are beneficial for controlling the carrier concentration, work function, and bandgap of the carbon nanotubes, thereby influencing their electrical and photoelectrical performance [17,18]. For example, Zhang and his team prepared fully printed flexible carbon nanotube photodetectors via plasma treatment, which exhibited a pronounced photothermal effect under laser illumination and displayed gate-voltage-dependent photoresponse characteristics. Specifically, when a positive gate voltage was applied, the photodetector exhibited semiconducting behavior (increasing conductivity with rising temperature), whereas it showed metallic behavior (decreasing conductivity with rising temperature) under a negative gate voltage, due to different temperature dependencies of carrier concentration and mobility. Further, the photothermal effect enhanced the responsivity to 1.1×10^{-3} A/W, which is 6.5 times higher than that of devices using a silicon substrate, primarily due to the low thermal conductivity of the plastic substrate, which accentuates the photothermal effect [19].

Another method to enhance the photoresponse of carbon nanotubes is through gradient illumination, which involves a change in light intensity from strong to weak. This variation can produce different carrier concentration gradients, thereby increasing the diffusion current, which is directly proportional to the carrier concentration gradient. For instance, Wu and his team explored the photoresponse of carbon nanotubes under different light intensities, finding that gradient illumination could significantly increase the diffusion current, a crucial factor for enhancing the efficiency of photoelectrical devices [20]. Additionally, gradient illumination can also induce a photothermal effect, creating a temperature gradient and thermovoltage within the carbon nanotubes, thus further enhancing the photoresponse [21].

In this study, we aim to synergistically enhance the photovoltage and photocurrent of buckypaper (BP) by integrating an optimized plasma gradient modification process with gradient illumination. BP, a macroscopic film composed of randomly oriented CNTs,

offers flexibility, scalability, and ease of fabrication while exhibiting the superior nanoscale properties of CNTs on a macroscopic scale [22–26]. We utilized argon plasma to treat the BP surface for varying durations, thereby creating carrier concentration gradients on BP. Subsequently, we measured the photovoltage and photocurrent of BP under uniform full illumination and gradient illumination, comparing the effects of different plasma power levels, gas types, and modification methods. Our findings reveal that BP subjected to gradient plasma modification combined with gradient illumination exhibited the highest photovoltage, and we discuss the potential mechanisms underlying this phenomenon.

2. Experimental Procedure

To prepare flexible buckypaper (BP), we utilized multi-walled carbon nanotubes (MWCNTs) acquired from CONJUTEK, product model CRUDE (CONJUTEK, Taipei City, Taiwan), which possess a purity greater than 95%. These MWCNTs have diameters ranging from 10 to 50 nanometers and lengths between 10 and 100 µm. To overcome the van der Waals forces causing mutual attraction among carbon nanotubes and to achieve uniform dispersion in the solution, we employed a methodical approach. Initially, we combined 0.06 g of carbon nanotube powder with 6 g of the surfactant Triton X-100 (EMPEROR Chemical Co., LTD, Taipei City, Taiwan) in a 500 mL beaker. Subsequently, deionized water was added until the total volume reached 500 mL. This mixture was then subjected to ultrasonication at a power of 100 W for 30 min, achieving preliminary dispersion.

For further refinement, the 500 mL solution was evenly distributed into ten separate beakers. Each beaker was then topped up with deionized water to a final volume of 500 mL. Following this dilution, each beaker underwent an additional ultrasonication process at a power of 50 W for 10 min. This step ensured that every single carbon nanotube was uniformly dispersed throughout the liquid.

Subsequently, the dispersion was subjected to vacuum filtration. Using a vacuum pump, the liquid was passed through filter paper, resulting in the collection of BP on the paper. The resultant BP film was then carefully peeled off from the filter paper and immersed in ethanol for two hours, followed by an additional hour of immersion in deionized water. This dual soaking process was employed to eliminate any residual Triton X. Finally, the BP was air-dried in a desiccator for 24 h to ensure complete removal of moisture.

The final product was a flexible BP with a weight of 0.06 g, a diameter of 4.5 cm, a thickness of 0.075 mm, and a porosity of 78%, as illustrated in Figure 1. For subsequent experimentation, the BP was cut into rectangular strips measuring 2.0 cm by 0.5 cm. These strips were then subjected to various experimental conditions for plasma treatment and optoelectronic measurement.

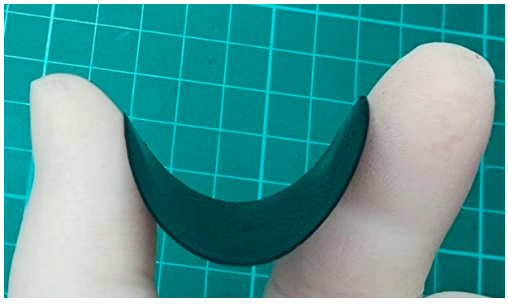

Figure 1. Using the vacuum filtration method to fabricate flexible thin sheets from multi-walled carbon nanotubes.

To enhance the optoelectronic response of buckypaper (BP), we employed a gas ion plasma treatment system (Junsun Tech. CS-400, New Taipei City, Taiwan). The experimental parameters for the plasma treatment are detailed as follows: the type of gas used was varied among argon, nitrogen, and oxygen. The working gas pressure was maintained at a constant 30 mTorr, and the gas flow rate was fixed at 20 standard cubic centimeters

per minute (SCCM). The plasma power was varied across different levels—5 W, 10 W, 20 W, 30 W, and 50 W. Within each sample, distinct regions were demarcated and subjected to plasma modification for different durations of 1 min, 2 min, 3 min, or 4 min, thereby creating gradients in carrier concentration.

For the measurement of the BP samples' optoelectronic properties, we utilized a solar simulator (A.M. 1.5 G Forter Tech. LCS-100, Taichung City, Taiwan). This simulator features a standard AM 1.5 G spectrum and an adjustable irradiance range of 0 to 1500 W/m^2. Silver paste was used to affix electrode wires onto the BP samples, which were then connected to a Keithley 2000 digital multimeter (Cleveland, OH, USA) to measure photovoltage and photocurrent.

The illumination modes were categorized into uniform full illumination and gradient illumination. Under uniform full illumination, the entire surface of the BP sample was exposed to the light source. For gradient illumination, we placed a gradient neutral density filter at the exit of the light source to achieve a gradually diminishing light intensity across the BP sample, ranging from high to low intensity. This gradient in light intensity consequently created varying carrier concentration gradients.

Moreover, based on the directions of the p-type carrier concentration gradients induced by both plasma modification and gradient illumination, we classified the gradient illumination modes into forward and reverse gradients. The forward gradient mode aligns the direction of the illumination gradient with the plasma gradient, while the reverse gradient mode opposes it. The schematic diagram illustrating these modes is depicted in Figure 2.

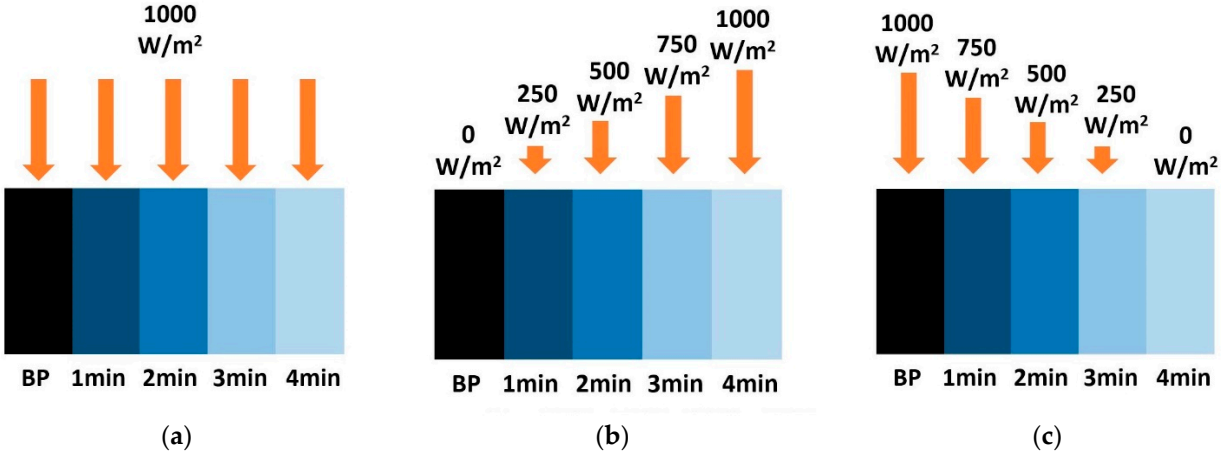

Figure 2. Illuminating a gradient plasma-modified BP with a light source using (**a**) uniform illumination, (**b**) forward gradient illumination, or (**c**) reverse gradient illumination.

To validate the variations in carrier concentration resulting from different plasma treatment durations or varying levels of illumination, we employed a Hall measurement system (Keithlink Tech., Taipei City, Taiwan). Utilizing the van der Pauw method, we conducted four-point probe measurements to ascertain the carrier concentration in the BP samples. Upon post-treatment with argon plasma at varying power levels, we observed slight modifications in the surface morphology, which were examined using a Field Emission Scanning Electron Microscope (FESEM, JEOL JSM-7000F, Tokyo, Japan).

To delve deeper into the changes in surface defects of the carbon nanotubes following plasma modification, we utilized Raman spectroscopy (Andor BWII RAMaker SR-750, Andor Technology Ltd., Belfast, UK). The BP samples were placed on glass slides and scanned with a laser beam at an excitation wavelength of 532 nm. The Raman spectroscopic analysis was performed by measuring the intensity and wavelength of the scattered light to detect alterations in the nanotube surface.

3. Results and Discussion

To verify that the carrier concentration of untreated buckypaper (BP) changes under illumination, we manually adjusted the solar simulator to output different light intensities.

The BP samples were uniformly illuminated and the carrier concentration was measured using the Hall effect method under various light intensities, specifically at 0, 250, 500, 750, 1000, and 1500 W/m^2. The results are presented in Figure 3a.

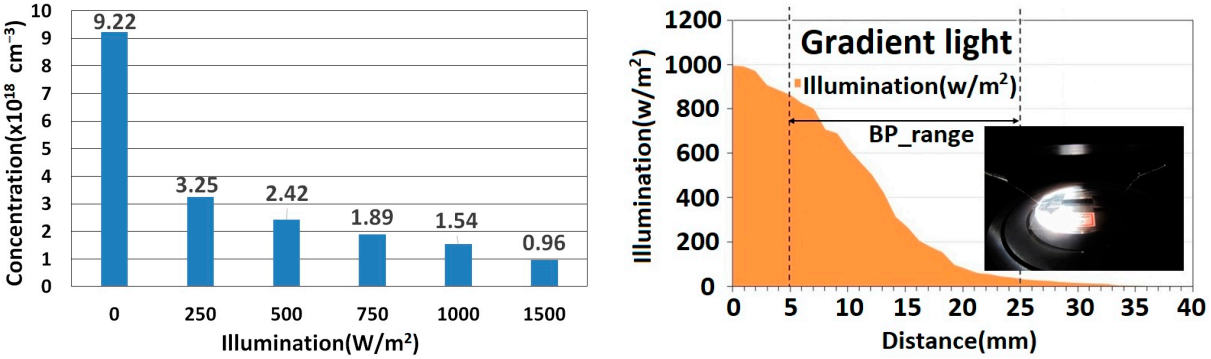

Figure 3. (**a**) Measured carrier concentrations of pure buckypaper in darkness and under uniform illumination at intensities of 250, 500, 750, 1000, and 1500 W/m^2. (**b**) Gradual changes in light intensity on buckypaper with varying distances.

Untreated BP exhibited p-type semiconductor behavior, indicating that holes are the predominant carriers. As the light intensity increased, the carrier concentration decreased from 9.22 $\times$ 10^{18} cm^{-3} at 0 W/m^2 to 0.96 $\times$ 10^{18} cm^{-3} at 1500 W/m^2. This decline is likely due to the recombination of photoinduced electron–hole pairs, which reduces the number of free carriers in the BP.

Subsequently, we introduced a gradient neutral density filter in front of the light source to produce a gradient light, aiming to enhance the sample's photoelectric response. We then carefully moved the light intensity sensor to detect the variation in light intensity across the gradient as a function of distance, as illustrated in Figure 3b.

To further enhance the optoelectronic properties of buckypaper (BP), we experimented with surface modification using argon plasma at a power setting of 20 W. Initially, the first sample underwent uniform plasma treatment for 1 min, followed by measurement of its carrier concentration. We repeated these steps with additional samples, varying the plasma treatment duration to 2 min, 3 min, and 4 min, respectively. The carrier concentrations for each sample are illustrated in Figure 4.

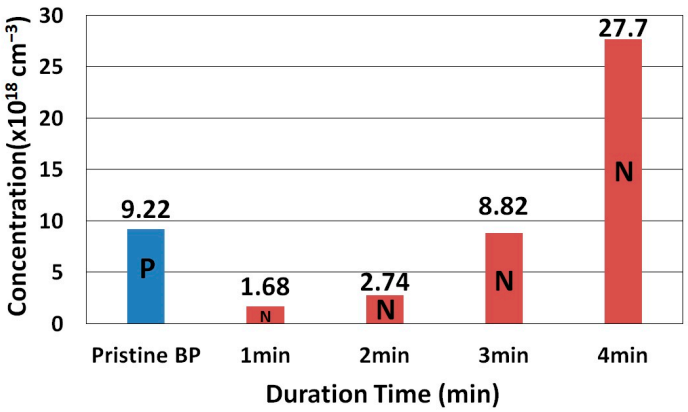

Figure 4. Changes in carrier concentration of BP under 20 W argon plasma treatment over different durations.

Our observations indicate that as the plasma treatment duration increased, the carrier concentration transitioned from p-type to n-type, becoming progressively more concentrated. This transition is hypothesized to result from the gradual depletion of oxygen

molecules bonded to the dangling bonds on the surface of the carbon nanotubes, caused by the prolonged exposure to plasma. This phenomenon effectively alters the BP's semiconducting properties to exhibit n-type behavior [27].

Furthermore, we varied the plasma power while maintaining a consistent treatment duration of one minute for each sample, aiming to modify the BP surface. The Raman spectra for these samples are shown in Figure 5. The D-band, G-band, and 2D-band peaks became progressively less sharp as the power increased, indicating a broadening effect. Such broadening is typically attributed to alterations in the material's structural or chemical properties.

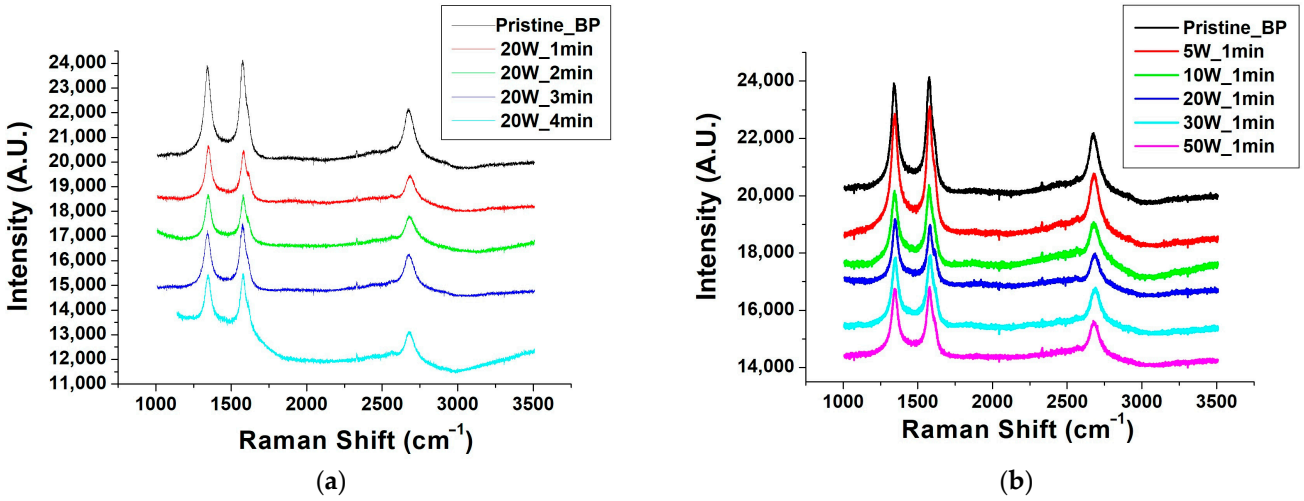

Figure 5. Raman spectra of buckypaper (BP) under (**a**) 20 W argon plasma power at various treatment durations and (**b**) different plasma powers for a one-minute argon plasma treatment.

The D-band is commonly associated with the presence of defects within the material, while the G-band serves as an indicator of the graphitization level in carbon materials. The 2D-band, being a secondary scattering process of the G-band, can provide insights into interlayer interactions and multilayer structures.

As the plasma power increased, the introduction of additional defects or changes to the chemical structure of the carbon nanotube surface likely caused the observed broadening and decrease in peak intensity. This can be attributed to the fact that higher-power plasma treatments tend to induce surface functionalization, introducing new functional groups or disrupting the existing structure of the carbon nanotubes.

In Raman spectroscopy, broadening of peaks may indicate an increase in structural disorder, which is associated with the introduction of defects. An increase in defects and irregular structures can lead to greater scattering of energy, resulting in broader peaks. Additionally, if the plasma treatment partially disrupts the graphitic structure, variations in the G-band peak shape might be observed.

Furthermore, if plasma treatment causes cross-linking between carbon nanotubes or the formation of new carbon-based structures, it could also impact the 2D-band. These structural changes would alter the electronic interactions between carbon nanotubes, thereby affecting the characteristics of the 2D-band.

In summary, the changes observed in the Raman spectra are likely due to structural defects, surface functionalization, or the disruption of the material structure induced by high-power argon plasma treatment [28,29]. These findings underscore the critical importance of plasma treatment conditions in modulating the properties of carbon-based materials.

Following our preliminary findings that plasma modification can induce changes in carrier concentration, we proceeded to experiment with three different plasma gases: argon, nitrogen, and oxygen. The plasma power was maintained at a constant 20 W, and the treatment duration was varied to 1 min, 2 min, 3 min, and 4 min. Each segment of the BP surface underwent plasma gradient modification across consecutive spatial regions. We

then measured the photovoltage and photocurrent under both uniform full illumination and forward gradient illumination conditions.

As depicted in Figure 6a–d, it is evident that the photovoltage and photocurrent of BP samples under gradient illumination were significantly higher than those under uniform illumination. Referring to the current density equation in semiconductor materials (Equation (1)), the total current density is the sum of the drift current and the diffusion current. When illuminated, numerous conductive electrons and holes are excited, and they contribute to the drift current $J_{p,drift}$ by moving under the influence of the built-in electric field. Additionally, the gradient in carrier concentration leads to an increase in dp/dx, the spatial derivative of the carrier concentration, which consequently enhances the diffusion current $J_{p,diffusion}$. Therefore, the overall current increases.

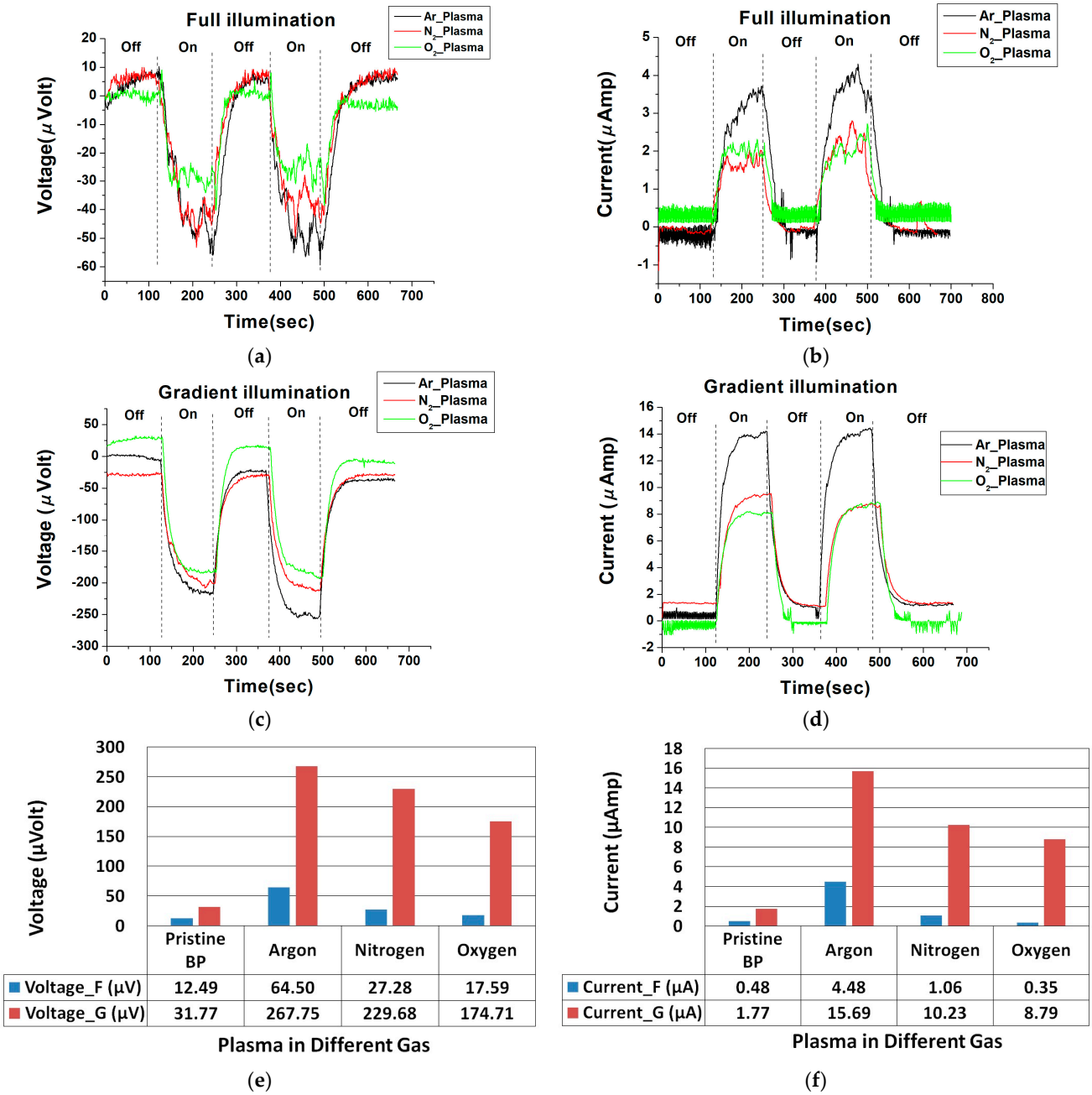

Figure 6. Photovoltage and photocurrent switching response diagrams for different plasma gases under uniform illumination mode in (**a**,**b**), and under gradient illumination mode in (**c**,**d**), with (**e**,**f**) providing comparative overview diagrams.

In summary, the higher photoelectric response observed under gradient illumination is attributed to the creation of a significant concentration gradient within the BP, which enhances the diffusion current of carriers. Simultaneously, the mechanism underlying the photoelectric effect in BP under uniform illumination can be explained by the vibrations of the π-bonds and the mobility of π-electrons within the CNTs when exposed to light.

$$J_p = J_{p,drift} + J_{p,diffusion} = qp\mu_p E - qD_p \frac{dp}{dx} \quad (1)$$

In this equation, $J_{p,drift}$ represents the drift current, $J_{p,diffusion}$ denotes the diffusion current, q is the elementary charge of the carrier, p indicates the concentration of the carriers, μ_p is the mobility of the carriers, E represents the electric field applied across the semiconductor material, and D_p is the diffusion coefficient for the carriers.

Additionally, under both uniform full illumination and gradient illumination conditions, the BP modified with argon (Ar) plasma exhibited the highest photovoltage, followed by the BP modified with nitrogen (N_2) plasma, while the BP modified with oxygen (O_2) plasma demonstrated the lowest photovoltage. This disparity can be attributed to the distinct effects of different plasma gases on the BP surface.

Ar plasma, being inert, primarily causes physical sputtering and etching of the BP surface. This process generates more defects and increases the surface area, thereby enhancing light absorption and carrier generation. In contrast, N_2 plasma can incorporate nitrogen atoms into the BP surface, forming C-N bonds and doping the BP with n-type impurities, which increases the electron concentration and conductivity. Meanwhile, O_2 plasma tends to oxidize the BP surface, forming C-O and C=O bonds and doping the BP with p-type impurities, which, in turn, reduces the electron concentration and conductivity.

Therefore, Ar plasma modification more effectively enhances the optoelectronic properties of BP compared to N_2 and O_2 plasma modifications. Based on these findings, Ar plasma was chosen as the optimal gas for BP modification. We subsequently employed different power settings—5 W, 10 W, 20 W, 30 W, and 50 W—with a treatment duration of one minute to modify the BP. The photovoltage and photocurrent responses under both uniform illumination and gradient illumination for these different power settings are depicted in Figure 7.

We tend to create more defects observed that BP modified with a plasma power of 20 W exhibited the highest photovoltage and photocurrent under both uniform full illumination and gradient illumination modes. This was followed by BP modified with 30 W plasma power, while BP modified with 50 W plasma power showed the lowest photovoltage and photocurrent. This phenomenon can be explained by the balance between plasma etching and plasma damage effects.

Plasma etching and increase the surface area of BP, which enhances light absorption and carrier generation. On the other hand, plasma damage can break C-C bonds and reduce the π-electron density in BP, thereby diminishing light absorption and carrier generation. As plasma power increases, the plasma etching effect becomes more pronounced, but so does the plasma damage effect. Therefore, an optimal plasma power exists that maximizes the plasma etching effects while minimizing plasma damage effects to achieve the best optoelectronic performance of BP. In this study, the optimal plasma power was found to be 20 W.

To further examine the damage induced by plasma bombardment on the BP surface, we utilized a Scanning Electron Microscope (SEM) to assess the impact of plasma power on BP's surface morphology. SEM images of BP treated with 20 W and 50 W Ar plasma are shown in Figure 8.

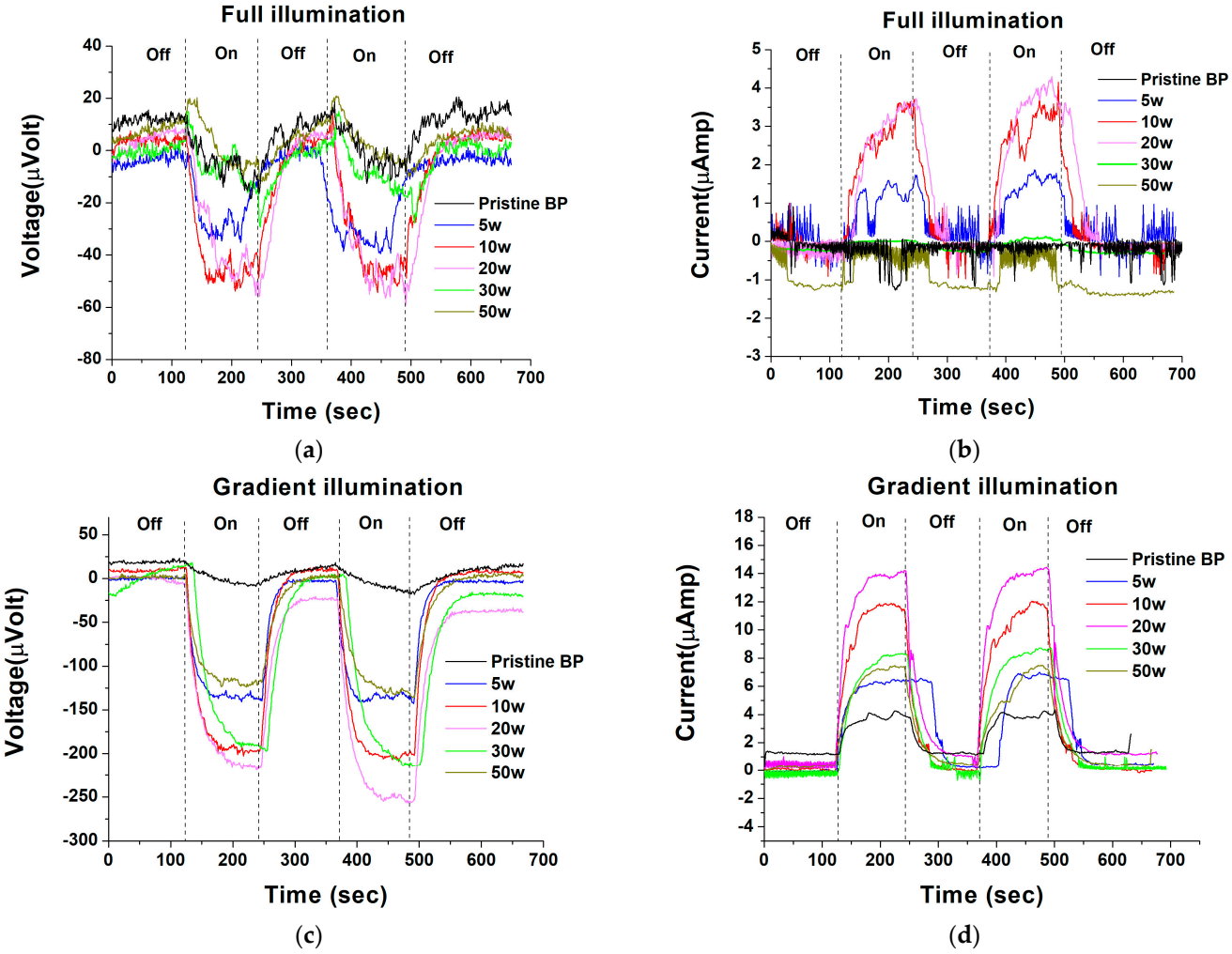

Figure 7. Photovoltage and photocurrent responses of buckypaper treated with plasma at different wattages, under (**a**,**b**) uniform illumination and (**c**,**d**) gradient illumination.

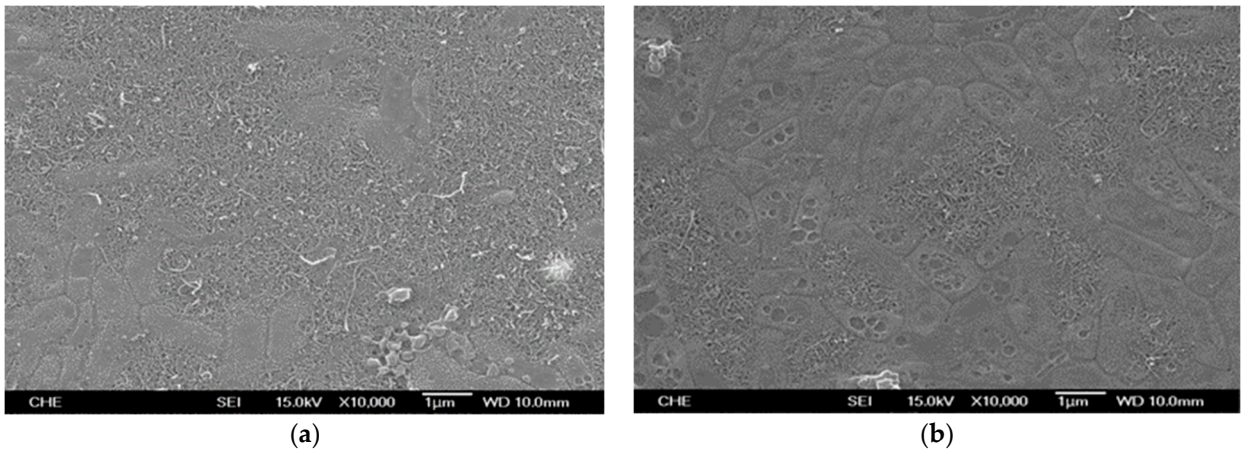

Figure 8. SEM images of buckypaper surfaces treated with argon plasma at (**a**) 20 watts and (**b**) 50 watts.

From Figure 8, it is evident that a plasma power of 50 W inflicted severe damage on the BP surface, leading to the fragmentation and localized collapse of carbon nanotubes, which subsequently fused together. This observation substantiates the plasma damage effect and elucidates why BP modified with 50 W plasma power exhibited poor optoelectronic performance. Conversely, a plasma power of 20 W did not cause significant damage to the

BP surface; instead, it created more defects and increased surface roughness. This supports the plasma etching effect and explains the enhanced optoelectronic performance of BP modified with 20 W plasma power.

Finally, using the experimental setup depicted in Figure 3, we applied a plasma power of 5 W to different spatial regions of a single BP sample. Each region was treated for varying durations of 1 min, 2 min, 3 min, or 4 min to induce carrier concentration gradients. Following the same experimental procedure, we repeated this with plasma powers of 10 W, 20 W, 30 W, and 50 W, each applied to different regions for different durations. These gradient-modified samples were then subjected to measurements of photovoltage under uniform illumination (Voltage_F), photovoltage under forward gradient illumination where the light gradient aligns with the plasma treatment gradient (Voltage_G_Forward), and photovoltage under reverse gradient illumination where the light gradient opposes the plasma treatment gradient (Voltage_G_Reverse).

From Figure 9, we can observe the experimental setup as depicted in Figure 2b. Assuming the positive direction is defined as rightward, the light intensity increases gradually from left to right. According to the p-type carrier concentration distribution shown in Figure 3a, the concentration decreases to the right, indicating $\frac{dp}{dx} < 0$. Additionally, the plasma gradient time increases from left to right. Based on the n-type carrier concentration distribution illustrated in Figure 4, the concentration increases to the right, resulting in $\frac{dn}{dx} > 0$, which equivalently means $\frac{dp}{dx} < 0$. When the illumination gradient aligns with the plasma gradient, the diffusion current and drift current can sum up, leading to higher photovoltage and photocurrent. Consequently, the photovoltage and photocurrent are higher when the gradients of illumination and plasma are in the same direction compared to when they are in opposite directions.

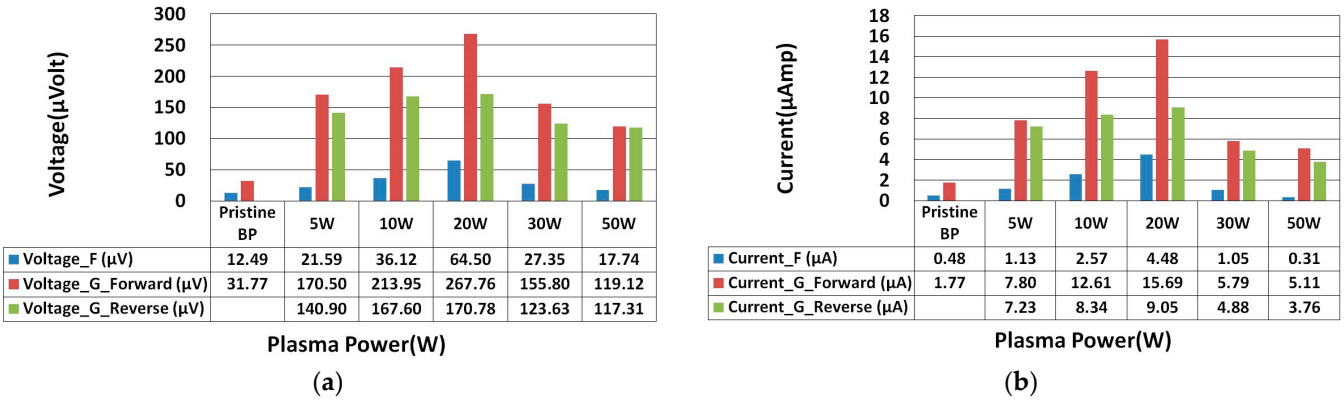

Figure 9. Comprehensive comparison of (**a**) photovoltage and (**b**) photocurrent of buckypaper treated with plasma gradients under uniform full illumination, forward gradient light, and reverse gradient light.

Comparatively, under uniform illumination, the intrinsic BP produced a photovoltage of 12.49 microvolts. After being modified by 20 W plasma under uniform illumination, the photovoltage increased to 64.50 microvolts. Furthermore, with the addition of plasma gradient modification and gradient illumination, the photovoltage reached 267.76 microvolts, which represents a 21.44 times increase. Similarly, the photocurrent rose from 0.48 microamps to 15.69 microamps, achieving a 32.69 times enhancement.

Finally, we attempted to compare the photoelectric voltage results generated by different experimental methods for enhancing BP photoelectric voltage, as listed in Table 1 below. Clearly, gradient plasma and gradient illumination can effectively enhance larger photoelectric voltage values.

Table 1. Comparison table of the photoelectric voltage of carbon nanotube paper before and after modification to enhance its photoelectric voltage using different experimental methods.

Methodology	By Gradient Plasma and Illumination		By ZnO Doping and Annealing [13]		By Ag Nanoparticle Doping [14]	
Enhancement	**Before**	**After**	**Before**	**After**	**Before**	**After**
Photovoltage (microvolt)	12.49	267.76	18.30	74.49	10.12	23.26

4. Conclusions

In this study, we identified argon as the optimal plasma modification gas. The power setting providing the best surface modification for BP was found to be 20 W. Additionally, by integrating plasma gradient modification and gradient illumination, we successfully fabricated flexible optoelectronic materials that demonstrated a significantly higher photoresponse.

Despite the advantageous properties of plasma-modified optoelectronic materials, such as enhanced flexibility compared to traditional rigid solid-state photodetectors, the increased surface area and multiple dangling bonds can lead to a slight self-charging effect. It is conceivable that improving the conductivity during the modification process could accelerate the charge–discharge recovery time, thereby optimizing the characteristics of flexible optoelectronic materials.

We believe that the enhanced extensibility, lightweight nature, and improved optoelectronic performance of these plasma-modified materials indicate their potential for diverse applications in solar cells and photodetection devices.

Author Contributions: Methodology, C.-C.Y., P.-Y.S., H.-Y.M., C.-Y.H., S.-H.L., J.-H.W., L.S. and J.-H.L.; writing—review and editing, J.-H.L. All authors have read and agreed to the published version of the manuscript.

Funding: This research was funded by Tunghai University and the National Science and Technology Council, Taiwan, R.O.C., grant number NSTC 112-2622-E-029-007.

Data Availability Statement: Data are contained within the article.

Conflicts of Interest: The authors declare no conflicts of interest.

References

1. Lijima, S. Helical microtubules of graphitic carbon. *Nature* **1991**, *354*, 56–58.
2. Popov, V.N. Carbon nanotubes: Properties and application. *Mater. Sci. Eng. R Rep.* **2004**, *43*, 61–102. [CrossRef]
3. Wang, F.; Matsuda, K. Applications of carbon nanotubes in solar cells. In *Nanocarbons for Energy Conversion: Supramolecular Approaches*; Springer: Cham, Switzerland, 2019; pp. 497–536.
4. Schroeder, V.; Savagatrup, S.; He, M.; Lin, S.; Swager, T.M. Carbon nanotube chemical sensors. *Chem. Rev.* **2018**, *119*, 599–663. [CrossRef] [PubMed]
5. Liu, J.H.; Huang, Y.S. Development of Microwave Filters with Tunable Frequency and Flexibility Using Carbon Nanotube Paper. *Nanomaterials* **2023**, *13*, 2497. [CrossRef]
6. Wei, D.; Liu, Y.; Cao, L.; Zhang, H.; Huang, L.; Yu, G. Synthesis and photoelectric properties of coaxial Schottky junctions of ZnS and carbon nanotubes. *Chem. Mater.* **2010**, *22*, 288–293. [CrossRef]
7. Itkis, M.E.; Borondics, F.; Yu, A.; Haddon, R.C. Bolometric infrared photoresponse of suspended single-walled carbon nanotube films. *Science* **2006**, *312*, 413–416. [CrossRef] [PubMed]
8. Saoudi, M.; Zaidi, B.; Alotaibi, A.A.; Althobaiti, M.G.; Alosime, E.M.; Ajjel, R. Polyaniline: Doping and functionalization with single walled carbon nanotubes for photovoltaic and photocatalytic application. *Polymers* **2021**, *13*, 2595. [CrossRef]
9. Cai, X.; Wang, S.; Peng, L.M. Recent progress of photodetector based on carbon nanotube film and application in optoe-lectronic integration. *Nano Res. Energy* **2023**, *2*, e9120058. [CrossRef]
10. Habisreutinger, S.N.; Blackburn, J.L. Carbon nanotubes in high-performance perovskite photovoltaics and other emerging optoelectronic applications. *J. Appl. Phys.* **2021**, *129*, 010903. [CrossRef]
11. Zaidi, B.; Smida, N.; Althobaiti, M.G.; Aldajani, A.G.; Almdhaibri, S.D. Polymer/carbon nanotube based nanocomposites for photovoltaic application: Functionalization, structural, and optical properties. *Polymers* **2022**, *14*, 1093. [CrossRef]
12. Miao, H.Y.; Liu, J.H.; Saravanan, L.; Wang, L.C.; Waychen, T. Photocurrent generation of TiO_2 and CuO doped MWCNT buckypaper. *Asian J. Chem.* **2013**, *25*, S9.

13. Liu, J.H.; Shen, P.Y. Heat-Annealed Zinc Oxide on Flexible Carbon Nanotube Paper and Exposed to Gradient Light to Enhance Its Photoelectric Response. *Nanomaterials* **2024**, *14*, 792. [CrossRef]
14. Zheng, Y.; Li, X.; Zhou, J.; Qin, Y.; Deng, Y.; Wang, Y. Boosted photothermoelectric effect in silver nanoparticles decorated carbon nanotube films for infrared detection and actuation. *Carbon* **2024**, *219*, 118810. [CrossRef]
15. Vohrer, U.; Zschoerper, N.P.; Koehne, Y.; Langowski, S.; Oehr, C. Plasma modification of carbon nanotubes and bucky papers. *Plasma Process. Polym.* **2007**, *4* (Suppl. S1), S871–S877. [CrossRef]
16. Xu, T.; Yang, J.; Liu, J.; Fu, Q. Surface modification of multi-walled carbon nanotubes by O_2 plasma. *Appl. Surf. Sci.* **2007**, *253*, 8945–8951. [CrossRef]
17. Allen, A.; Cannon, A.; Lee, J.; King, W.P.; Graham, S. Flexible microdevices based on carbon nanotubes. *J. Micromech. Microeng.* **2006**, *16*, 2722. [CrossRef]
18. Nasibulin, A.G.; Pikhitsa, P.V.; Jiang, H.; Brown, D.P.; Krasheninnikov, A.V.; Anisimov, A.S.; Kauppinen, E.I. A novel hybrid carbon material. *Nat. Nanotechnol.* **2007**, *2*, 156–161. [CrossRef]
19. Zhang, S.; Cai, L.; Wang, T.; Miao, J.; Sepúlveda, N.; Wang, C. Fully printed flexible carbon nanotube photodetectors. *Appl. Phys. Lett.* **2017**, *110*, 123105. [CrossRef]
20. Wu, W.; Yang, F.; Fang, X.; Cai, X.; Liu, X.; Zhang, F.; Wang, S. Ultrafast carbon nanotube photodetectors with bandwidth over 60 GHz. *ACS Photonics* **2023**, *10*, 1060–1069. [CrossRef]
21. Chani MT, S.; Karimov, K.S.; Asiri, A.M.; Ahmed, N.; Bashir, M.M.; Khan, S.B.; Azum, N. Temperature gradient measurements by using thermoelectric effect in CNTs-silicone adhesive composite. *PLoS ONE* **2014**, *9*, e95287.
22. Li, W.; Wang, X.; Chen, Z.; Waje, M.; Yan. Carbon nanotube film by filtration as cathode catalyst support for pro-ton-exchange membrane fuel cell. *Langmuir* **2005**, *21*, 9386–9389. [CrossRef]
23. Sinnott, S.B.; Andrews, R. Carbon nanotubes: Synthesis, properties, and applications. *Crit. Rev. Solid State Mate-Rials Sci.* **2001**, *26*, 145–249. [CrossRef]
24. Anzar, N.; Hasan, R.; Tyagi, M.; Yadav, N.; Narang, J. Carbon nanotube—A review on Synthesis, Properties and plethora of applications in the field of biomedical science. *Sens. Int.* **2020**, *1*, 100003. [CrossRef]
25. Hirotani, J.; Ohno, Y. Carbon nanotube thin films for high-performance flexible electronics applications. In *Single-Walled Carbon Nanotubes: Preparation, Properties and Applications*; Springer: Berlin/Heidelberg, Germany, 2019; pp. 257–270.
26. Jo, A.; Chung, S.I.; Kim, P.K.; Lee, J.W.; Lee, H.J.; Yang, H.J.; Park, J.H. All-printed paper-based micro-supercapacitors using water-based additive-free oxidized single-walled carbon nanotube pastes. *ACS Appl. Energy Mater.* **2021**, *4*, 13666–13675. [CrossRef]
27. Derycke, V.; Martel, R.; Appenzeller, J.; Avouris, P. Controlling doping and carrier injection in carbon nanotube transistors. *Appl. Phys. Lett.* **2002**, *80*, 2773–2775. [CrossRef]
28. Yung, C.S.; Tomlin, N.A.; Heuerman, K.; Keller, M.W.; White, M.G.; Stephens, M.; Lehman, J.H. Plasma modification of vertically aligned carbon nanotubes: Superhydrophobic surfaces with ultra-low reflectance. *Carbon* **2018**, *127*, 195–201. [CrossRef]
29. Jorio, A.; Saito, R. Raman spectroscopy for carbon nanotube applications. *J. Appl. Phys.* **2021**, *129*, 021102. [CrossRef]